PERGAMON

Journal of the Mechanics and Physics of Solids
49 (2001) 785–811

JOURNAL OF THE
MECHANICS AND
PHYSICS OF SOLIDS

www.elsevier.com/locate/jmps

Multi-axial electrical switching of a ferroelectric: theory versus experiment

J.E. Huber, N.A. Fleck*

Department of Engineering, University of Cambridge, Trumpington Street, Cambridge CB2 1PZ, UK

Received 5 May 2000; received in revised form 4 August 2000

Abstract

Samples of the polycrystalline ferroelectric ceramic PZT-5H were poled by applying an electric field at room temperature. Subsequently, an electric field was applied to the samples at a range of angles to the poling direction. The measured non-linear responses in electric displacement are used to construct "yield surfaces" in electric field space corresponding to the onset of ferroelectric switching. The results are compared with predictions from three models: (i) a previous self-consistent polycrystal calculation with rate-independent, non-hardening crystal plasticity; (ii) a simplified crystal plasticity model with viscoplastic (rate-dependent) behaviour and a sufficient number of transformation systems to reproduce the polycrystalline behaviour; (iii) a phenomenological model based on rate-independent flow theory, using kinematic hardening and a quadratic yield surface in electric field and stress space. The experiments suggest that the self-consistent crystal plasticity formulation is most able to reproduce the multi-axial electrical response and yield surface of the polycrystal. The phenomenological model is able to reproduce the uniaxial response accurately, but gives relatively poor performance for multi-axial loading paths, in its present form. A tolerable compromise in multi-axial modelling is the simplified crystal plasticity approach. This is able to reproduce multi-axial constitutive behaviour with reasonable accuracy, whilst offering computational simplicity and speed similar to that of the phenomenological model.
© 2001 Elsevier Science Ltd. All rights reserved.

Keywords: B. Ferroelectric material; A. Twinning; B. Crystal plasticity; B. Constitutive behaviour

1. Introduction

Modelling the non-linear constitutive response of ferroelectrics presents a tough challenge. The materials typically exhibit electro-mechanical coupling, hysteresis, memory

* Corresponding author. Tel.: +44-1223-332650; fax: +44-1223-332662.
E-mail address: naf1@eng.cam.ac.uk (N.A. Fleck).

0022-5096/01/$ - see front matter © 2001 Elsevier Science Ltd. All rights reserved.
PII: S0022-5096(00)00052-1

effects, anisotropy, and saturation of strain and electric displacement; all of these effects serve to complicate the constitutive description. Nevertheless, a robust, accurate constitutive model is needed for the purposes of understanding manufacturing processes such as surface machining and the poling of ferroelectric actuators and sensors, predicting the behaviour of ferroelectric devices, and studying fatigue degradation and crack growth. The aim of the present paper is to compare the performance of three distinct modelling approaches with a view to selecting a constitutive model which is suitable for use in finite element studies of boundary value problems.

1.1. Ferroelectric switching

The key physical phenomenon governing the non-linear response of ferroelectrics below the Curie temperature is switching of the remnant electrical polarisation of crystalline material between distinct polarisation states. In the most commonly used ferroelectrics (doped alloys in the lead zirconate/lead titanate system) there exists a tetragonal phase with six distinct crystal variants and a rhombohedral phase with eight distinct crystal variants. When the remnant polarisation switches between distinct states, the switch is in some cases accompanied by a change of shape of the unit cell, giving rise to remnant strain. Consequently, switching may be driven by stress (termed ferroelastic switching) or by electric field. Commonly used ferroelectrics are random, sintered polycrystals and consequently there is a variety of crystallographic orientations present in a bulk sample; this has the effect of smearing out the macroscopic response of the polycrystal, compared to that of a single crystal.

1.2. Saturation of switching

Switching is the source of remnant strain and polarisation in ferroelectrics. When the applied loads (stress or electric field) can produce no further switching, the ferroelectric reaches a saturated state. Consider a random polycrystal, before poling. The orientations of the crystal variants are uniformly distributed over all spatial directions; this reference configuration has zero remnant strain and zero polarisation (Fig. 1a). Subsequent switching may produce polarisation and remnant strain, but note that the switching process conserves volume. Although the average remnant strain and polarisation in the reference configuration are zero, each crystal variant within the material is in a saturated local state with a polarisation of magnitude P in a direction $\mathbf{n}$, a remnant strain of $2e$ parallel to $\mathbf{n}$ and a remnant strain of $-e$ radially (perpendicular to $\mathbf{n}$).

In order to illustrate possible states of overall (macroscopic) saturation, consider three cases of loading applied to a random polycrystal in the reference configuration. First, consider a monotonically increasing electric field; this causes alignment of polarisation vectors along (or close to) the direction of the applied field. When saturation has been attained, an axisymmetric remnant strain and polarisation are present. In the limiting case where all crystal variants become fully aligned with the applied field, the polarisation reaches a magnitude P and the axial strain reaches $2e$, whilst the radial strain is $-e$ (Fig. 1b). Second, consider uniaxial tension applied to the polycrystal in

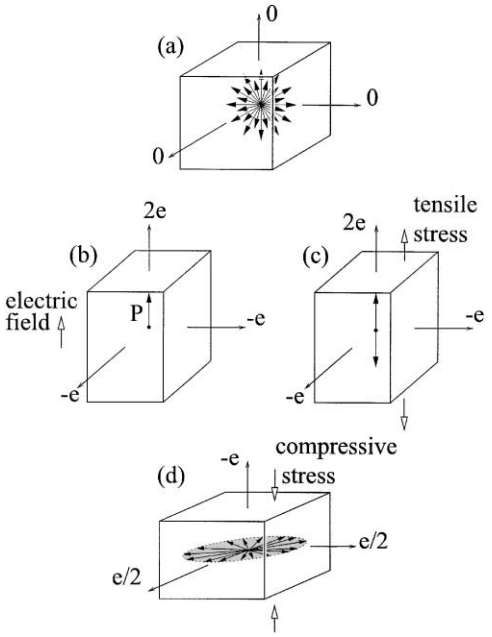

Fig. 1. (a) Reference state with polarisation vectors in all directions and zero net polarisation and strain. (b) Saturated state with polarisation P and axial remnant strain $2e$. (c) Saturated state with zero polarisation and axial remnant strain $2e$. (d) Saturated state with zero polarisation and $-e$ axial remnant strain.

the reference configuration. Switching causes an axisymmetric state of remnant strain, but by symmetry the polarisation remains zero. The saturated state of remnant strain is the same as that reached under electric field loading; the limiting case of full alignment is shown in Fig. 1c. Finally, consider uniaxial compression starting from the reference configuration. By symmetry, the average polarisation remains zero. Switching causes each crystal variant to orientate its long axis close to the transverse plane. In the limiting case where all variants have their long axis in the transverse plane, the remnant strain is $-e$ axially and $e/2$ radially (see Fig. 1d). Note that the saturation states shown in Fig. 1b–d share the common feature that the most negative principal strain has a value of $-e$.

The limiting cases of saturation shown in Fig. 1b–d are not observed in ferroelectric polycrystals in practice because of restrictions imposed by particular crystal systems. For experimental measurements of saturation under uniaxial loading, see Lynch (1996).

1.3. Multi-axial switching models

By incorporating the above features into a switching model, Hwang et al. (1995) were able to reproduce the main effects found in the macroscopic response of ferroelectric polycrystals, namely: dielectric hysteresis, butterfly hysteresis in strain versus

applied electric field, and mechanical nonlinearity. Hwang et al. (1995) argued that switching occurs when the work done by local fields during a given ferroelectric switching event exceeds a critical value. They used an averaging procedure to account for the variety of crystallographic orientations, and assumed uniform stress and electric fields. A comparison of the early model of Hwang et al. (1995) with measurements of uniaxial material response (Lynch, 1996; Cao and Evans, 1993) made evident a deficiency, in that the model neglected the local interaction between adjacent regions of material with differing polarisation states. This interaction was successfully incorporated by Arlt (1996) in the context of dielectric hysteresis, and subsequently in the coupled context by Hwang et al. (1998), Chen and Lynch (1998a,b), Chen et al. (1997) and Huber et al. (1999). These models differ in detail, but all essentially use a switching criterion based on the energy released during the switching event or the thermodynamic driving force, and use a micromechanical approach to account for local interactions. Models of this type reproduce reasonably accurately the uniaxial material response, when calibrated against test data. The model of Huber et al. (1999) will be tested here against a multi-axial experiment. The modelling approach described above, using crystal switching (or crystal plasticity), requires a large number of internal variables designed to keep track of the polarisation state of different regions of the polycrystal (or equivalently, the volume fractions corresponding to a variety of polarisation directions). The incorporation of such a constitutive model at each Gauss point within a finite element analysis is feasible, but results in a high level of computational complexity.

1.4. Background to a simplified crystal plasticity model

The desire for a simple formulation which captures quantitatively the key aspects of ferroelectric behaviour motivates the introduction of a second model, also based on crystal plasticity. Instead of using the particular set of crystal transformation systems corresponding to single-crystal behaviour, with a homogenisation scheme to account for the variety of crystallographic orientations, this second model employs an artificially chosen, representative set of transformation systems, designed to reproduce the macroscopic behaviour of the polycrystal without reproducing the details of particular crystal structures. This approach is unable to account for the subtle distinctions between switching in, for example, a rhombohedral crystal system and a tetragonal crystal system. However, in modelling the macroscopic response of a polycrystal, this distinction is thought to be minor (Hwang et al., 1998). This simplified crystal plasticity approach uses a viscoplastic formulation to avoid the difficulty encountered in rate-independent crystal plasticity of solving for the set of instantaneously active transformation systems (active slip systems in classical crystal plasticity). In the viscoplastic formulation all transformation systems are simultaneously active, and yielding corresponds to an increased rate of transformation. The use of a rate-dependent model of this type is consistent with the observed time-dependent relaxation behaviour of ferroelectric polycrystals. The macroscopic saturation of switching can be captured by reducing the rate of transformation of each system as the corresponding volume fraction of material to be transformed approaches zero.

1.5. Phenomenological theories of switching

An alternative approach, with the potential for a simple and robust model, is phenomenological theory. An early attempt to model the macroscopic response of ferroelectrics to applied fields in this way was made by Chen (1980) and Chen and Madsen (1981). Their work uses a single scalar internal state variable which represents the extent of alignment of dipoles; the evolution laws for the internal state variable are chosen to produce the best fit to experimental data. Thus, the model is able to reproduce the uniaxial dielectric hysteresis and butterfly hysteresis of a given ferroelectric material, provided that the fitting functions are correctly chosen. A detailed account of the thermodynamic structure of phenomenological models for ferroelectricity is given by Bassiouny et al. (1988a,b) and Bassiouny and Maugin (1989a,b). Their thermodynamic formulation uses the concept of internal variables to capture the dependence of the material state upon loading history, and introduces a yield function (or "loading function") which defines the domain of reversible behaviour within the space of applied loads. They also introduce isotropic and kinematic hardening, representing enlargement and translation of the yield surface, respectively. A practical constitutive model can be developed around this framework by defining a Gibbs (or Helmholtz) free energy function. From this function, strain and electric displacement are derived (or stress and electric field in the case of a Helmholtz function). The coefficients of the thermodynamic energy function are measurable material parameters (elastic, dielectric and piezoelectric moduli and so forth). In choosing the form of the thermodynamic energy function it is desirable to include sufficient terms to capture all significant material effects, whilst minimising the number of independent coefficients that must be determined experimentally.

Despite the apparent simplicity of the phenomenological approach, few attempts have been made to realise a practical phenomenological model for the constitutive response of ferroelectrics until recently. Cocks and McMeeking (1999) have developed a phenomenological model which simulates the non-linear response of ferroelectrics to electrical and mechanical loading. Their model is formulated in a uniaxial form but is readily extended to multi-axial loading. It uses the average state of remnant strain and remnant electric polarisation in the polycrystal as internal state variables. Similarly, Kamlah and Tsakmakis (1999) use the remnant strain and polarisation as internal variables. However, they decompose the remnant strain into two parts. One part is due to the remnant polarisation, and is associated with orienting the long axis of crystal unit cells along a particular direction; the other part is due to ferroelastic switching and is not related to the macroscopic polarisation. In this way, Kamlah and Tsakmakis recognise the underlying connection between remnant polarisation and remnant strain, in that both can occur as the consequence of a single ferroelectric switching event. It should be noted that the connection between remnant polarisation and remnant strain becomes most significant when the polycrystal is close to a state of saturation of one or other remnant quantity. For example, when the saturation polarisation is reached, there is necessarily an accompanying remnant strain. The one-dimensional model of Kamlah and Tsakmakis has recently been extended to allow multi-axial loading (Kamlah and Böhle, 2001). The connection between remnant strain and polarisation is also discussed

by Lynch (1998), who uses two scalar variables (α, β) corresponding to the extent of remnant strain and polarisation, with coupling to capture the way in which remnant strain and polarisation interact. Lynch develops a one-dimensional phenomenological model by proposing functional relations between the applied loads and the internal variables (α, β); hysteresis is incorporated by switching to different functions during unloading. Landis and McMeeking (1999) have developed a phenomenological model for the uncoupled problem of ferroelastic switching which accounts for the material response close to saturation by introducing internal variables corresponding to the principal remnant strains. Using these variables, Landis and McMeeking are able to account for effects of the saturation of ferroelastic switching during multi-axial loading paths. Fan et al. (1999) model a range of soft and hard PZT ceramics in one dimension using three Maxwell-type elements in parallel. Each element consists of a non-linear spring and a frictional slider. The similarity between the stress–strain and stress–electric displacement responses is exploited to give a single model which captures both. A phenomenological model drawing on several features from the work described above is presented here. It is designed to capture the best features from previous phenomenological models, whilst remaining sufficiently simple to be well suited to incorporation into a finite element analysis.

In the following sections, three models are discussed in detail: (i) a previous self-consistent polycrystal calculation with rate-independent, non-hardening crystal plasticity (Huber et al., 1999); (ii) a simplified crystal plasticity model with viscoplastic (rate-dependent) behaviour and a sufficient number of transformation systems to reproduce the polycrystalline behaviour; (iii) a phenomenological model based on rate-independent flow theory, using kinematic hardening and a quadratic yield surface in electric field and stress space. Their responses are calibrated to give a near fit to measurements of the response of a ferroelectric polycrystal to uniaxial loading with electric field. A multi-axial experiment is described; this consists of polarising initially unpoled material using electric field only, followed by electric field loading in a different direction. The predictions of each model for the material response in multi-axial electrical loading are then compared with the measured responses.

2. Crystal plasticity models

The self-consistent model of Huber et al. (1999) will be used here for the purposes of comparison. It represents a crystal plasticity theory which accounts for progressive switching by domain wall motion within crystals; the theory assumes that several distinct ferroelectric switching mechanisms may operate simultaneously. In the present section, a simplified crystal plasticity model is presented. A nearly isotropic single crystal with a particular set of transformation systems is assumed.

We begin by summarising the governing field equations for a ferroelectric. Consider a ferroelectric solid at constant temperature below the Curie point. The solid is taken to be in equilibrium mechanically and electrically. Newton's and Maxwell's laws give

$$\nabla \cdot \boldsymbol{\sigma} + \mathbf{f} = 0, \quad \nabla \cdot \mathbf{D} - q = 0, \tag{1}$$

where $\boldsymbol{\sigma}$ is the stress field, $\mathbf{f}$ is the body force distribution, $\mathbf{D}$ is the electric displacement and q is the free charge density. The following notation is adopted throughout. First- and higher-order tensor quantities appear in bold; appropriate tensor products are evident from the context in most instances, and are otherwise made explicit using indicial notation. Quasi-static and small strain conditions are assumed so that

$$\mathbf{E} = -\nabla \Phi, \quad e\boldsymbol{\varepsilon} = (\nabla \mathbf{u} + (\nabla \mathbf{u})^{\mathrm{T}})/2, \tag{2}$$

where $\mathbf{E}$ is the electric field, derived from the scalar electric potential Φ, and $\boldsymbol{\varepsilon}$ is the strain, derived from the displacement field $\mathbf{u}$.

By decomposing strain and electric displacement into recoverable (linear) and remnant parts, the constitutive response of the ferroelectric solid may be written as

$$\begin{bmatrix} \boldsymbol{\varepsilon} \\ \mathbf{D} \end{bmatrix} = \begin{bmatrix} \mathbf{S} & \mathbf{d} \\ \mathbf{d} & \boldsymbol{\kappa} \end{bmatrix} \begin{bmatrix} \boldsymbol{\sigma} \\ \mathbf{E} \end{bmatrix} + \begin{bmatrix} \boldsymbol{\varepsilon}_{\mathrm{r}} \\ \mathbf{P}_{\mathrm{r}} \end{bmatrix}, \tag{3}$$

where $\mathbf{S}$, $\mathbf{d}$ and $\boldsymbol{\kappa}$ are the tensors of elastic modulus, piezoelectric modulus and dielectric permittivity, respectively; $\boldsymbol{\varepsilon}_{\mathrm{r}}$ and $\mathbf{P}_{\mathrm{r}}$ are the remnant (or, by analogy with crystal plasticity theory, "plastic") parts of strain and electric displacement. The quantities $\boldsymbol{\varepsilon}_{\mathrm{r}}$ and $\mathbf{P}_{\mathrm{r}}$ are taken to be due entirely to ferroelectric switching. Note that the moduli $\mathbf{S}$, $\mathbf{d}$ and $\boldsymbol{\kappa}$ may not remain constant during ferroelectric switching; ferroelectric domains are anisotropic and local changes in polarisation orientation during switching give rise to changes in the macroscopic moduli. The constitutive relation (3) may be inverted to the form

$$\begin{bmatrix} \boldsymbol{\sigma} \\ \mathbf{E} \end{bmatrix} = \begin{bmatrix} \mathbf{C} & -\mathbf{h} \\ -\mathbf{h} & \boldsymbol{\beta} \end{bmatrix} \begin{bmatrix} \boldsymbol{\varepsilon} - \boldsymbol{\varepsilon}_{\mathrm{r}} \\ \mathbf{D} - \mathbf{P}_{\mathrm{r}} \end{bmatrix}, \tag{4}$$

where the tensors $(\mathbf{C}, \mathbf{h}, \boldsymbol{\beta})$ are related directly to $(\mathbf{S}, \mathbf{d}, \boldsymbol{\kappa})$ by tensor inversion. The solid is taken to be composed entirely of ferroelectric crystals. Within each crystal, a single crystallographic orientation exists. However, there may be distinct regions of the crystal (domains) with differing polarisation states, and consequently different local values of $\mathbf{S}$, $\mathbf{d}$ and $\boldsymbol{\kappa}$. Let the number of distinct crystal variants present in a given crystal be M and the volume fraction of the crystal occupied by the Ith variant be c_I. It is assumed that the stress and electric field are uniform within a given crystal. It is further assumed that the quantities $\boldsymbol{\varepsilon}$, $\boldsymbol{\varepsilon}_{\mathrm{r}}$, $\mathbf{D}$, and $\mathbf{P}_{\mathrm{r}}$ for the crystal may be represented by the corresponding volume averages over the crystal. Thus in a crystal containing M distinct crystal variants,

$$\begin{bmatrix} \boldsymbol{\varepsilon} \\ \mathbf{D} \end{bmatrix} = \sum_{I=1}^{M} \begin{bmatrix} \mathbf{S}_I & \mathbf{d}_I \\ \mathbf{d}_I & \boldsymbol{\kappa}_I \end{bmatrix} \begin{bmatrix} \boldsymbol{\sigma} \\ \mathbf{E} \end{bmatrix} c_I + \begin{bmatrix} \boldsymbol{\varepsilon}_{\mathrm{r}} \\ \mathbf{P}_{\mathrm{r}} \end{bmatrix}. \tag{5}$$

Here, $\mathbf{S}_I$, $\mathbf{d}_I$, and $\boldsymbol{\kappa}_I$ are the tensors of elastic, piezoelectric and dielectric modulus of the Ith crystal variant. Ferroelectric switching on transformation system α occurs by the movement of a domain wall, transferring volume fraction from variant J to variant I at a rate $\dot{f}_\alpha$. The crystal system under consideration has M crystal variants and N transformation systems. Note that a transformation system for which $c_J = 0$ has reached saturation and is effectively "locked" so that $\dot{f}_\alpha = 0$ on such a system.

Define $\boldsymbol{\varepsilon}_I$ and $\mathbf{p}_I$ as the remnant strain and polarisation in the Ith crystal variant. In practical examples, the magnitudes $|\mathbf{p}_I|$ are identical whilst the three invariants of $\boldsymbol{\varepsilon}_I$ are equal to those of $\boldsymbol{\varepsilon}_J$ for all I and J. The volume averages of remnant strain and polarisation are given by

$$\begin{bmatrix} \boldsymbol{\varepsilon}_{\mathrm{r}} \\ \mathbf{P}_{\mathrm{r}} \end{bmatrix} = \sum_{I=1}^{M} c_I \begin{bmatrix} \boldsymbol{\varepsilon}_I \\ \mathbf{p}_I \end{bmatrix}. \tag{6}$$

Increments in the average state of remnant strain and polarisation of the crystal are due entirely to ferroelectric transformation, so that

$$\begin{bmatrix} \dot{\boldsymbol{\varepsilon}}_{\mathrm{r}} \\ \dot{\mathbf{P}}_{\mathrm{r}} \end{bmatrix} = \sum_{I=1}^{M} \dot{c}_I \begin{bmatrix} \boldsymbol{\varepsilon}_I \\ \mathbf{p}_I \end{bmatrix} = \sum_{\alpha=1}^{N} \dot{f}_\alpha \begin{bmatrix} \boldsymbol{\mu}_\alpha \gamma_\alpha \\ \mathbf{s}_\alpha P_\alpha \end{bmatrix}, \tag{7}$$

where $\boldsymbol{\mu}_\alpha$ is identical to the Schmid orientation tensor, while $\mathbf{s}_\alpha$ is a unit vector in the direction of the change in remnant polarisation. The scalars γ_α and P_α define the maximum shear strain and polarisation change due to the transformation system α.

Huber et al. (1999) show that the dissipated work rate $\dot{w}_{\mathrm{D}}$ due to transformations on all systems within a given crystal may be written as

$$\dot{w}_{\mathrm{D}} = \sum_{\alpha} G_\alpha \dot{f}_\alpha, \tag{8}$$

where G_α is the thermodynamic driving force for transformation on slip system α given by

$$G_\alpha = [\boldsymbol{\sigma} \quad \mathbf{E}] \begin{bmatrix} \boldsymbol{\mu}_\alpha \gamma_\alpha \\ \mathbf{s}_\alpha P_\alpha \end{bmatrix} + \frac{1}{2} [\boldsymbol{\sigma} \quad \mathbf{E}] \begin{bmatrix} \Delta \mathbf{S}_\alpha & \Delta \mathbf{d}_\alpha \\ \Delta \mathbf{d}_\alpha & \Delta \boldsymbol{\kappa}_\alpha \end{bmatrix} \begin{bmatrix} \boldsymbol{\sigma} \\ \mathbf{E} \end{bmatrix}. \tag{9}$$

Here $\Delta \mathbf{S}_\alpha \equiv \mathbf{S}_I - \mathbf{S}_J$ where system α transforms material from variant J to variant I; $\Delta \mathbf{d}_\alpha$ and $\Delta \boldsymbol{\kappa}_\alpha$ are defined similarly. A piezoelectric tensor of the form

$$d_{ijk} = (d_{33}) n_i n_j n_k + (d_{31})(n_i \delta_{jk} - n_i n_j n_k) + \tfrac{1}{2}(d_{15})(\delta_{ij} n_k - 2 n_i n_j n_k + \delta_{ik} n_j) \tag{10}$$

is adopted for each variant, where d_{33}, d_{31} and d_{15} are crystal constants and $\mathbf{n}$ is a unit vector in the polarisation direction of the variant. For commonly used ferroelectric crystals the anisotropy in the elastic and dielectric moduli is relatively small compared to that of the piezoelectric moduli. Neglecting terms in $\Delta \mathbf{S}_\alpha$ and $\Delta \boldsymbol{\kappa}_\alpha$ gives

$$G_\alpha = \boldsymbol{\sigma} \cdot \boldsymbol{\mu}_\alpha \gamma_\alpha + \mathbf{E} \cdot \mathbf{s}_\alpha P_\alpha + \boldsymbol{\sigma} \cdot \Delta \mathbf{d}_\alpha \cdot \mathbf{E}. \tag{11}$$

When G_α attains a critical value G_{c}, transformation is expected to occur on system α. Up to this point, the description of the single crystal matches that given by Huber et al. (1999). There, the analysis continues with a derivation of the instantaneous tangent moduli of the crystal, assuming rate-independent behaviour and a hardening rule. Calculations using the rate-independent model of Huber et al. (1999), with a self-consistent averaging scheme to account for varying crystal orientations, are presented in Section 5. That approach necessitates an iterative scheme to solve for the transformation rates $\dot{f}_\alpha$, which adds a level of computational complexity to the constitutive model. A simpler approach, which allows direct evaluation of $\dot{f}_\alpha$, is to assume

viscoplastic behaviour with a power law relationship between the driving force G_α and the corresponding transformation rate $\dot{f}_\alpha$. The viscoplastic constitutive law must allow for saturation of transformation system α when the volume fraction c_I of the transforming crystal variant approaches zero. The following viscoplastic law is proposed:

$$\dot{f}_\alpha = \dot{f}_0 \left| \frac{G_\alpha}{G_c} \right|^{(m-1)} \frac{G_\alpha}{G_c} \left(\frac{c_I}{c_0} \right)^{(1/k)}. \tag{12}$$

With $m \gg 1$, G_c becomes the critical value of G_α at which there is a rapid increase in transformation rate. The volume fraction c_I controls saturation of transformation system α; when $c_I = 0$, system α is saturated. The state with all $c_I = c_0$ corresponds to an initial, unpoled condition, where all variants have equal volume fraction. The transformation rate $\dot{f}_0$ corresponds to the conditions $G_\alpha = G_c$ and $c_I = c_0$. Perfectly plastic behaviour with sudden "lock-up" at the point of saturation is reproduced in the limit $m, k \to \infty$. By choosing a sufficiently small value for k, such as $k \approx 1$, it is possible to reproduce the gradual onset of saturation which is characteristic of polycrystalline ferroelectrics. Implementation of the above constitutive relations is straightforward when the loads at time t are specified as $(\boldsymbol{\sigma}(t), \mathbf{E}(t))$. A representative set of crystal variants and transformation systems must be chosen, along with an initial state for the volume fractions c_I. Since we assume uniform stress and electric field, the driving force G_α may be evaluated for each transformation system α directly, and hence the transformation rates $\dot{f}_\alpha$. With the values $\dot{f}_\alpha$ in hand, volume fractions c_I and all other variables may be updated. Provided that reasonably small time increments δt are used, the response $(\boldsymbol{\varepsilon}(t), \mathbf{D}(t))$ can be calculated accurately. Direct integration in this way is sufficiently rapid and accurate to allow the constitutive response of the model to be explored. For finite element analysis, the rate tangent formulation of Pierce et al. (1984) can be used.

The modelling parameters which must be specified are γ_α, P_α, G_c, $\dot{f}_0$, m, k. These parameters may be fixed by fitting the model response to measurements of the material response under low-frequency cyclic electric field loading. The parameters γ_α and P_α control the remnant strain and polarisation, respectively, at saturation; once γ_α and P_α have been fixed, the remaining four parameters may be varied over a wide range without significantly affecting the magnitude of the strain and polarisation hysteresis. For a given set of transformation systems, with known values of $\mathbf{p}_I$ and $\boldsymbol{\varepsilon}_I$, the values of P_α and γ_α can be determined directly. The width of the dielectric hysteresis loop, which is approximately twice the coercive field strength of the material, is controlled by G_c. The shape of the $\mathbf{P}_r$ versus $\mathbf{E}$ response at the onset of ferroelectric switching is controlled by m; high values of m correspond to a sudden onset of switching and *vice versa*. Similarly, k controls the onset of saturation. The product mk controls the peak value of the slope $\partial \mathbf{D}/\partial \mathbf{E}$ during ferroelectric switching under electric field loading.

2.1. Transformation systems

The viscoplastic behaviour described above could be used for a single crystal with any particular set of transformation systems. Here, the aim is to introduce a set of transformation systems which reproduce the isotropic response of a random polycrystal. In

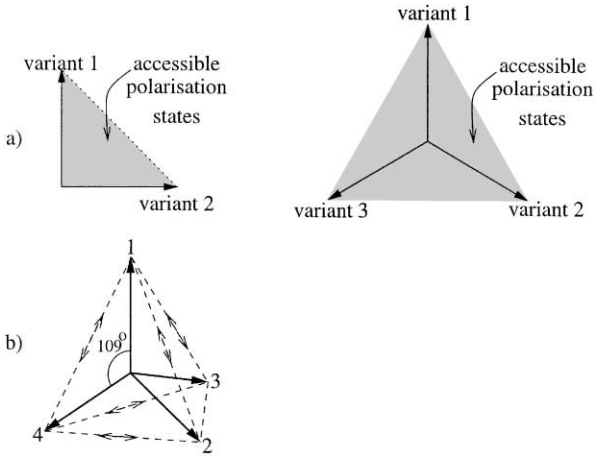

Fig. 2. (a) In two dimensions, three variants are needed so that all polarisation directions are accessible. (b) In three dimensions, four crystal variants in a regular tetrahedral arrangement allow all polarisation directions, and give rise to six transformation systems.

a random polycrystal there are many transformation systems, such that the characteristic tensors $\boldsymbol{\mu}_\alpha$ and $\mathbf{s}_\alpha$ are uniformly distributed over all spatial directions. We wish to invent a simple set of crystal variants and transformation systems which achieve a sufficiently uniform distribution of $\boldsymbol{\mu}_\alpha$ and $\mathbf{s}_\alpha$. From an initial state in which all variants have equal volume fractions, the response should ideally be isotropic. With a small number of transformation systems, the aim is to achieve a response which varies by no more than a few percent when the direction of applied field is varied. It is also necessary to arrange the crystal variants such that by combining positive volume fractions $0 \leq c_I \leq 1$, the volume average polarisation can lie in any direction. Fig. 2 shows that in a two-dimensional space it is necessary to have at least three distinct crystal variants in order to achieve this. In a three-dimensional space, at least four distinct crystal variants are necessary. With only four crystal variants, the most uniform arrangement is to set the polarisation directions $\mathbf{p}_I$ to correspond to the vertices of a regular tetrahedron centred on the origin (see Fig. 2).

A crystal with these four variants has six transformation systems, with the six $\mathbf{s}_\alpha$ directions corresponding to the edges of the tetrahedron. This choice of crystal variants has some practical relevance: the transformation systems in the tetrahedral arrangement correspond exactly to the 109° transformation systems in rhombohedral ferroelectrics. Is a single three-dimensional crystal with only four variants sufficiently isotropic for our purposes? Clearly, the answer is no (see Fig. 3): the magnitude of polarisation at saturation varies by a factor of 3 depending on the direction of applied electric field.

A substantial improvement in the degree of isotropy can be made by averaging over five sets of four variants in the tetrahedral arrangement, orientated such that the polarisation directions of the resulting 20 crystal variants correspond to the vertices

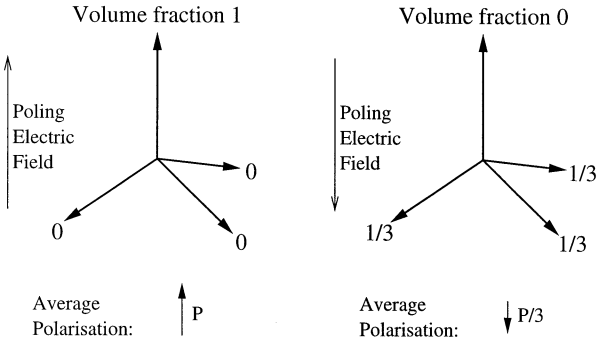

Fig. 3. The saturation polarisation in a single crystal with the tetrahedral arrangement of variants depends strongly on the direction of the applied poling field.

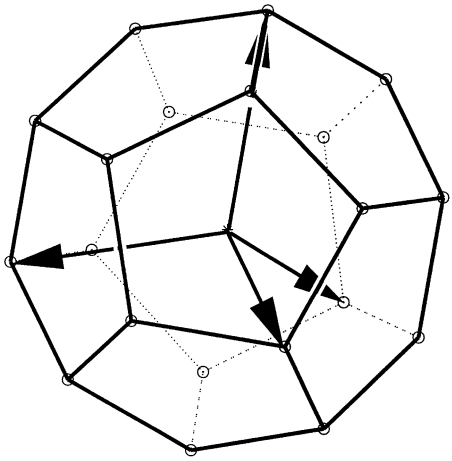

Fig. 4. Twenty polarisation directions in a regular dodecahedral arrangement (marked "○") and one subset of four variants in the tetrahedral arrangement (marked with arrows).

of a regular dodecahedron. The arrangement of the 20 polarisation states, and one subset of four variants in the tetrahedral arrangement are shown in Fig. 4. Each set of four tetrahedrally arranged variants gives six transformation systems, so there are 30 transformation systems in total.

The extent of anisotropy in this arrangement can be measured by considering electric field loading in two extreme cases: (a) $\mathbf{E}$ is aligned with the polarisation direction $\mathbf{p}_I$ of one of the crystal variants (i.e. $\mathbf{E}$ is directed to a vertex of the dodecahedron); (b) $\mathbf{E}$ makes an angle 37.4° with the nearest $\mathbf{p}_I$ (i.e. $\mathbf{E}$ is directed to the centre of a face of the dodecahedron). The saturation polarisation in case (a) is $71\%|\mathbf{p}_I|$ and in case (b) is $79\%|\mathbf{p}_I|$. The dodecahedral arrangement is a compromise with reasonably good isotropy and a small number of transformation systems. (Note that to achieve

repeatability to within 5% using randomly chosen crystallographic orientations, Hwang et al. (1998) use 5000 crystals.)

3. Rate-independent phenomenological model

In this section, a phenomenological theory for the non-linear response of ferroelectrics is developed, with the one-dimensional model of Cocks and McMeeking (1999) as the starting point. The aim is to simplify modelling by using fewer internal variables than the crystal plasticity approach. Internal variables are required because the material response depends both on the current loads and on the history of ferroelectric switching. In the crystal plasticity approach, scalar internal variables corresponding to the volume fractions of each crystal variant have been introduced; in the present phenomenological model, the average remnant strain $\boldsymbol{\varepsilon}_r$ and polarisation $\mathbf{P}_r$ are used as the internal variables. From symmetry arguments it is easy to show that neither $\boldsymbol{\varepsilon}_r$ nor $\mathbf{P}_r$ alone can characterise the internal state of the ferroelectric material. For example, consider purely mechanical loading with a uniaxial compressive stress from the unpoled isotropic state ($\mathbf{P}_r = 0$, $\boldsymbol{\varepsilon}_r = 0$). By symmetry, $\mathbf{P}_r$ remains at zero throughout and so cannot be used to track the changes in internal state which give rise to saturation of switching. A similar argument can be used to show that $\boldsymbol{\varepsilon}_r$ alone is not sufficient to determine the state of the piezoelectric modulus, as follows. Consider two specimens, in the isotropic state. Apply an electric field $\mathbf{E}(t)$ to the first specimen, causing ferroelectric switching, such that it develops a piezoelectric modulus $\mathbf{d}$ and remnant strain $\boldsymbol{\varepsilon}_r$. Now apply exactly the opposite electric field loading $-\mathbf{E}(t)$ to the second specimen. By symmetry, it will develop the same state of remnant strain $\boldsymbol{\varepsilon}_r$ as the first specimen, but its piezoelectric modulus will be $-\mathbf{d}$. The difference in piezoelectric moduli cannot be accounted for using internal variable $\boldsymbol{\varepsilon}_r$ alone. Thus neither $\boldsymbol{\varepsilon}_r$ nor $\mathbf{P}_r$ is individually sufficient as an internal variable.

Fundamental choices in setting up a phenomenological theory are whether to use a deformation theory or a flow theory, a hardening or a non-hardening model, and if hardening, whether it be isotropic hardening, kinematic hardening, or a combination of the two. The aim is to choose the simplest structure which captures the main effects, rather than the most general structure, which may be computationally cumbersome.

Ferroelectrics display extensive hysteresis in the response to cyclic electrical and mechanical loading, and so a flow theory is desirable; this will allow for distinct branches of the response during loading and unloading. The crystal plasticity theory of Huber et al. (1999) considered the case of negligible hardening (a small hardening modulus was used for the purpose of numerical stability only). The absence of significant hardening is consistent with the steep slope $\partial\mathbf{D}/\partial\mathbf{E}$ of the electric displacement versus electric field curve during ferroelectric switching under an electric field. However, it is necessary to capture the saturation of switching. In the rate-independent crystal plasticity formulation of Huber et al. (1999) this was achieved by switching off transformation systems which reach saturation; effectively, these systems harden suddenly at the point of lock-up. In the viscoplastic formulation (12) there is a decrease in

transformation rate as saturation is approached. In the phenomenological model, it is desirable to include some form of hardening to capture the saturation of switching, but the form of hardening must give rise to stable cyclic hysteresis. This largely eliminates the choice of isotropic hardening in favour of kinematic hardening, following the approach of Cocks and McMeeking, (1999). In a kinematically hardening flow theory the yield surface translates in loading space, following the loading point. This suggests the presence of residual stresses or electric fields, which bias the loading surface, and is consistent with micromechanical considerations of the electrical and mechanical interactions between adjacent ferroelectric crystals. Residual stresses also arise naturally from thermodynamic considerations (Cocks and McMeeking, 1999), and are consistent with Bauschinger effects observed in ferroelectric polycrystals (Huber, 1998). Noting that the remnant strains due to ferroelectric switching are pure shears, we argue that the loading surface is a function of the deviatoric part of stress $\mathbf{s}$ where $s_{ij} \equiv \sigma_{ij} - \delta_{ij}\sigma_{kk}/3$. Chen (1980) notes that a hydrostatic stress can give rise to a non-linear response in some ferroelectric compositions. This, however, is due to phase transitions rather than ferroelectric domain wall motion, and is an effect which we neglect, limiting the present analysis to ferroelectric compositions in which domain wall motion is the dominant mechanism of ferroelectric transformation.

The general structure of the model, then, will consist of a yield surface, which defines the state of loading $(\mathbf{s}, \mathbf{E})$ that can give rise to a non-linear response, and evolution rules for the internal variables. Let the centre of the yield surface in deviatoric stress space and electric field space be $(\mathbf{s}_c, \mathbf{E}_c)$. Now define the deviation of the loading point $(\mathbf{s}, \mathbf{E})$ from the yield surface centre $(\mathbf{s}_c, \mathbf{E}_c)$ as

$$\begin{bmatrix} \hat{\mathbf{s}} \\ \hat{\mathbf{E}} \end{bmatrix} = \begin{bmatrix} \mathbf{s} - \mathbf{s}_c \\ \mathbf{E} - \mathbf{E}_c \end{bmatrix}. \tag{13}$$

Introduce a yield surface which is a function of $(\hat{\mathbf{s}}, \hat{\mathbf{E}})$ and of the internal variables $(\boldsymbol{\varepsilon}_r, \mathbf{P}_r)$ such that

$$G(\hat{\mathbf{s}}, \hat{\mathbf{E}}, \boldsymbol{\varepsilon}_r, \mathbf{P}_r) - G_c \leq 0, \tag{14}$$

where, in the absence of isotropic hardening, G_c remains constant. During yielding, equality applies in (14). The evolution of the yield surface centre $(\mathbf{s}_c, \mathbf{E}_c)$ is governed by the internal variables $(\boldsymbol{\varepsilon}_r, \mathbf{P}_r)$ and the kinematic hardening law is stated as

$$\begin{bmatrix} \dot{\mathbf{s}}_c \\ \dot{\mathbf{E}}_c \end{bmatrix} = [\mathbf{H}(\boldsymbol{\varepsilon}_r, \mathbf{P}_r)] \begin{bmatrix} \dot{\boldsymbol{\varepsilon}}_r \\ \dot{\mathbf{P}}_r \end{bmatrix}, \tag{15}$$

where $[\mathbf{H}(\boldsymbol{\varepsilon}_r, \mathbf{P}_r)]$ represents a set of hardening moduli, coupling $(\dot{\boldsymbol{\varepsilon}}_r, \dot{\mathbf{P}}_r)$ to $(\dot{\mathbf{s}}_c, \dot{\mathbf{E}}_c)$. It remains to define the evolution of $(\boldsymbol{\varepsilon}_r, \mathbf{P}_r)$; following conventional plasticity theory, a normality rule is used in conjunction with a convex yield surface $G = G_c$. Huber et al. (1999) note that normality and convexity do not follow directly from crystal plasticity considerations when the anisotropic nature of the linear elastic crystal properties is accounted for. This is because of the possibility of a switching system which transforms material from a crystal variant with high compliance to a crystal variant with low compliance, at constant load. Such a transformation would be accompanied by a release

of stored strain energy. In this case, the ferroelectric material could do work against a closed cycle of imposed loading, in violation of Drucker's postulate for stable materials. Simulations of ferroelectric switching using the model of Huber et al. (1999) indicate that neglecting compliance changes due to switching has only a minor effect on the response. This justifies the use of the normality rule as an approximation:

$$\begin{bmatrix} \dot{\boldsymbol{\varepsilon}}_r \\ \dot{\mathbf{P}}_r \end{bmatrix} = \dot{\lambda} \begin{bmatrix} \frac{\partial G}{\partial \boldsymbol{\sigma}} \\ \frac{\partial G}{\partial \mathbf{E}} \end{bmatrix}, \tag{16}$$

where $\dot{\lambda}$ is the (unknown) plastic multiplier, which, in the case of non-zero hardening, may be found as follows. For subsequent use, we introduce four derivatives of the yield function:

$$\mathbf{N} = \frac{\partial G}{\partial \boldsymbol{\sigma}} = \frac{\partial G}{\partial \hat{\mathbf{s}}}, \qquad \mathbf{n} = \frac{\partial G}{\partial \mathbf{E}} = \frac{\partial G}{\partial \hat{\mathbf{E}}}, \tag{17}$$

$$\mathbf{M} = \frac{\partial G}{\partial \boldsymbol{\varepsilon}_r}, \qquad \mathbf{m} = \frac{\partial G}{\partial \mathbf{P}_r}. \tag{18}$$

The consistency relation $\dot{G} = \dot{G}_c = 0$ during ferroelectric switching (no isotropic hardening) may then be expressed as

$$[\mathbf{N}\ \mathbf{n}] \begin{bmatrix} \dot{\hat{\mathbf{s}}} \\ \dot{\hat{\mathbf{E}}} \end{bmatrix} + [\mathbf{M}\ \mathbf{m}] \begin{bmatrix} \dot{\boldsymbol{\varepsilon}}_r \\ \dot{\mathbf{P}}_r \end{bmatrix} = 0. \tag{19}$$

Making use of Eqs. (13) and (15)–(19) allows the plastic multiplier $\dot{\lambda}$ to be written explicitly as

$$\dot{\lambda} = \frac{[\mathbf{N}\ \mathbf{n}] \begin{bmatrix} \dot{\mathbf{s}} \\ \dot{\mathbf{E}} \end{bmatrix}}{[\mathbf{N}\ \mathbf{n}][\mathbf{H}] \begin{bmatrix} \mathbf{N} \\ \mathbf{n} \end{bmatrix} - [\mathbf{M}\ \mathbf{m}] \begin{bmatrix} \mathbf{N} \\ \mathbf{n} \end{bmatrix}}. \tag{20}$$

Using the plastic multiplier, increments in the internal variables $(\boldsymbol{\varepsilon}_r, \mathbf{P}_r)$ and in $(\hat{\mathbf{s}}, \hat{\mathbf{E}})$ can be calculated for a given load increment $(\dot{\mathbf{s}}, \dot{\mathbf{E}})$. The increments $(\dot{\boldsymbol{\varepsilon}}_r, \dot{\mathbf{P}}_r)$ and $(\dot{\mathbf{s}}, \dot{\mathbf{E}})$ can be treated as Jaumann rates in order to take into account material spin. The material response to an imposed path of loading can be calculated by dividing the load path into a series of small increments.

3.1. Particular form of the phenomenological model

Now, consider particular choices of the yield function $G(\hat{\mathbf{s}}, \hat{\mathbf{E}}, \boldsymbol{\varepsilon}_r, \mathbf{P}_r)$ and the kinematic hardening functions $[\mathbf{H}(\boldsymbol{\varepsilon}_r, \mathbf{P}_r)]$. Since the solid is isotropic in the unpoled state, G is a function of at least the invariants of $\hat{\mathbf{s}}$ and the single invariant $|\hat{\mathbf{E}}|$ of $\hat{\mathbf{E}}$. Since the first invariant of $\hat{\mathbf{s}}$ is zero, the simplest approach is to use the second invariant $\hat{\mathbf{s}}_e = \sqrt{\frac{3}{2}\hat{\mathbf{s}} \cdot \hat{\mathbf{s}}}$ corresponding to the Mises effective stress. Indeed, a convex function $G^2 = \alpha \hat{\mathbf{s}}_e^2 + |\hat{\mathbf{E}}|^2$

was used by Cocks and McMeeking (1999), where the constant α is required for dimensional consistency. It is well known (see, for example, measurements by Lynch, 1996) that application of an electric field alone from the initially isotropic state can give rise to a remnant strain $\boldsymbol{\varepsilon}_r$ in ferroelectrics. In order to incorporate this effect in the phenomenological formulation it is necessary to include coupling between electrical and mechanical terms in either of G or [**H**]. Cocks and McMeeking (1999) placed the coupling in [**H**] by setting $\partial\dot{\mathbf{s}}_c/\partial\dot{\mathbf{P}}_r \neq 0$ and $\partial\dot{\mathbf{E}}_c/\partial\dot{\boldsymbol{\varepsilon}}_r \neq 0$. We introduce a coupled term $\hat{\mathbf{s}}\cdot\hat{\mathbf{E}}\mathbf{P}_r$ (in indicial notation $\hat{s}_{ij}\hat{E}_i P_{j(r)}$) to the phenomenological expression for G, with $\mathbf{P}_r$ introduced to ensure that this term is active whenever the material has remnant polarisation. The assumed expression for G then takes the form

$$G^2 = \alpha\hat{s}_e^2 + |\hat{\mathbf{E}}|^2 + \beta\hat{\mathbf{s}}\cdot\hat{\mathbf{E}}\mathbf{P}_r, \tag{21}$$

where β is a scalar parameter which will be used to provide a fit to measured material responses. Combining (21) with the normality rule gives non-zero values of $\dot{\boldsymbol{\varepsilon}}_r$ for loading with electric field only, provided $\mathbf{P}_r \neq 0$. At the point of transformation, a critical value of G is reached such that $G = G_c$.

It remains to specify the form of the hardening moduli represented by [**H**], which control the evolution of $(\mathbf{s}_c, \mathbf{E}_c)$. Since coupling is included in the form of the yield function G it is not necessary to include coupling in [**H**] and thus $\partial\dot{\mathbf{s}}_c/\partial\dot{\mathbf{P}}_r$ and $\partial\dot{\mathbf{E}}_c/\partial\dot{\boldsymbol{\varepsilon}}_r$ may be set to zero. Assuming a simple form of kinematic hardening in which $\partial\dot{\mathbf{s}}_c/\partial\dot{\boldsymbol{\varepsilon}}_r$ is a scalar function of $\boldsymbol{\varepsilon}_r$ only and $\partial\dot{\mathbf{E}}_c/\partial\dot{\mathbf{P}}_r$ is a scalar function of $\mathbf{P}_r$ only gives

$$\begin{bmatrix} \dot{\mathbf{s}}_c \\ \dot{\mathbf{E}}_c \end{bmatrix} = \begin{bmatrix} h_s(\boldsymbol{\varepsilon}_r) & 0 \\ 0 & h_e(\mathbf{P}_r) \end{bmatrix} \begin{bmatrix} \dot{\boldsymbol{\varepsilon}}_r \\ \dot{\mathbf{P}}_r \end{bmatrix}. \tag{22}$$

The scalar functions $h_s(\boldsymbol{\varepsilon}_r)$ and $h_e(\mathbf{P}_r)$ are chosen in such a way as to provide for rapid hardening when saturation is reached. The choice of the most suitable form of hardening for use in a phenomenological model remains an open question. The diagonal form of hardening is adopted in (22) for simplicity, and is adequate to describe the observed material behaviour under uniaxial loading.

The saturation condition must be described in terms of the remnant strain and remnant polarisation. There is a finite magnitude of polarisation P_{sat} corresponding to saturation, so the function h_e must increase rapidly as $|\mathbf{P}_r|/P_{sat}$ approaches unity. This requirement is satisfied by writing

$$h_e(\mathbf{P}_r) = h_{0e}\left(1 - \frac{|\mathbf{P}_r|}{P_{sat}}\right)^{-n_e}, \tag{23}$$

where h_{0e} is an initial hardening rate, and setting $n_e \gg 1$ gives rapid lock-up at the saturation point.

Saturation occurs, regardless of the value of $|\mathbf{P}_r|/P_{sat} < 1$, when the remnant strain tensor reaches a critical value. As discussed in the introduction, and as argued by Landis and McMeeking (1999), states of remnant strain corresponding to lock-up have the common feature that the most negative principal remnant strain ε_{rIII} takes on a fixed value, $-\varepsilon_{sat}$. For ε_{rIII} to reach $-\varepsilon_{sat}$ the crystal variants must be arranged such that no further compression can occur in the principal direction corresponding to ε_{pIII}, unless it be elastic compression. This can be realised in the model if $h_s(\boldsymbol{\varepsilon}_r)$ increases rapidly as

the lock-up condition is approached. Whilst it is straightforward to extract the principal remnant strains, a simple approximation to the saturation condition $\varepsilon_{\mathrm{rIII}} = -\varepsilon_{\mathrm{sat}}$ is given by

$$u \equiv \frac{I_2}{4}\left(3 - \left(\frac{I_3}{I_2}\right)^3\right) = \varepsilon_{\mathrm{sat}}, \tag{24}$$

where I_2 and I_3 are invariants of $\boldsymbol{\varepsilon}_{\mathrm{r}}$ given by

$$I_2 = (\tfrac{2}{3}\boldsymbol{\varepsilon}_{\mathrm{r}} \cdot \boldsymbol{\varepsilon}_{\mathrm{r}})^{(1/2)}, \qquad I_3 = (\tfrac{4}{3}\boldsymbol{\varepsilon}_{\mathrm{r}(ij)}\boldsymbol{\varepsilon}_{\mathrm{r}(jk)}\boldsymbol{\varepsilon}_{\mathrm{r}(ki)})^{(1/3)}. \tag{25}$$

In (25) the summation convention is applied to the bracketed indices. The condition $u = \varepsilon_{\mathrm{sat}}$ gives the saturation condition exactly for axisymmetric states of strain, and does so approximately otherwise.

A suitable functional form for h_{s}, similar to (23), may now be written

$$h_{\mathrm{s}}(\boldsymbol{\varepsilon}_{\mathrm{r}}) = h_{0\mathrm{s}}\left(1 - \frac{u}{\varepsilon_{\mathrm{sat}}}\right)^{-n_{\mathrm{s}}} \tag{26}$$

with $h_{0\mathrm{s}}$ being an initial hardening rate corresponding to $u = 0$, and with $n_{\mathrm{s}} \gg 1$ corresponding to rapid lock-up.

4. Experiment

A plate of unpoled, polycrystalline lead zirconate titanate (PZT-5H) of thickness 5 mm, prepared by the mixed oxide route, was supplied by Morgan Matroc Ltd.[1] A parent-specimen of size 18 mm × 18 mm × 5 mm was cut from the plate using a diamond saw. Conducting surface electrodes were made on the 18 mm × 18 mm faces by sputtering on gold followed by painting with a thin layer of silver electrode paint. The parent-specimen was clamped lightly between brass plates, under transformer oil, such that good electrical contact was made between the brass plates and the electroded surfaces. The specimen was then poled by application of an electric field of strength 1.5 M V m^{-1} at room temperature for 100 s. During poling, the remnant polarisation reached a value of 0.25 C m^{-2}. After poling, the surface electrodes were removed by polishing. Finally, the parent-specimen was cut using a diamond saw into cuboidal blocks, with the faces of the blocks cut at differing angles θ to the direction of remnant polarisation, as shown in Fig. 5.

The resulting specimens varied in size from 5 mm × 5 mm × 4 mm (cut at $\theta = 0^\circ$), to 3.5 mm × 3.5 mm × 4 mm (cut at $\theta = 45^\circ$). Four specimens were cut at each of $\theta = 0$, 15, 30°, and two specimens at $\theta = 45^\circ$, making a total of 14 blocks. On each specimen, pairs of faces were electroded by sputtering gold, and painting with silver electrode paint. The faces on which electrodes were made were chosen such that an electric field could be applied at angles of 0–180° to the remnant polarisation direction, in steps of 15° (13 specimens, with one spare 90° specimen for a repeatability check). Wire connections were soldered lightly to the electrodes. Each specimen was then

[1] Morgan Matroc Ltd., Unilator Division, Vauxhall Industrial Estate, Ruabon, Wrexham, LL14 6HY.

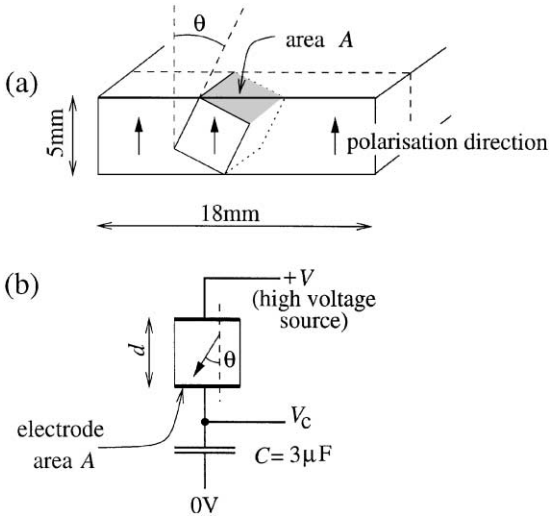

Fig. 5. Experimental arrangement: (a) cutting out of a block of poled material at angle θ; (b) applying electric field to the block and measuring surface charge.

suspended under oil and subjected to a loading path consisting of increasing the electric field strength from 0 to 1.5 $\mathrm{MV\,m^{-1}}$ and then decreasing back to zero, over a total time of 30 s. The oil used was a low conductivity transformer oil, but nevertheless allowed significant leakage currents. Leakage was measured in a separate test at several levels of applied field, and the experimental data presented here is corrected accordingly. The surface charge on each specimen was measured by the voltage across a 3 μF capacitor placed in series with the specimen (see Fig. 5). The total charge accumulated on the specimen electrodes was typically about 10^{-5} C, and thus the voltage across the metering capacitor did not exceed about 3.5 V, representing a disturbance to the applied electric field of 10^{-3} $\mathrm{MV\,m^{-1}}$ or 0.07% of the peak value of the applied electric field.

For each specimen the applied voltage V and the voltage across the metering capacitor V_c were sampled at 1 Hz and recorded. These data were subsequently converted into electric field E versus electric displacement D data, using $E=V/d$ and $D=CV_c/A$ where d is the distance between electrodes, C is the capacitance of the metering capacitor and A is the area of the electroded surface (see Fig. 5).

5. Results

Fig. 6 shows the change in electric displacement versus applied electric field for a selection of specimens at $\theta = 0, 45, 90, 135$ and 180°. The 0° specimen corresponds to the case where the applied electric field is in the same direction as the poling field; here there is only slight non-linearity in the dielectric response. By contrast, in the 180° specimen the applied field is in the opposite direction to the poling direction and a change of remnant polarisation occurs, of magnitude 0.48 $\mathrm{C\,m^{-2}}$. For the tests on the

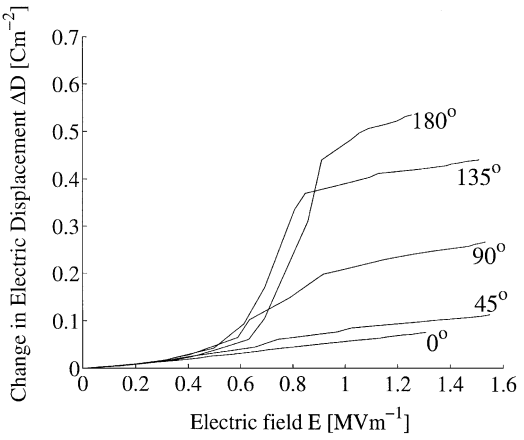

Fig. 6. Measured dielectric responses of specimens loaded with electric field at angle θ in the range 0–180° from the poling direction.

180 and 0° specimens, experimental data were captured in the range $E < 1.3\ \mathrm{MV\,m^{-1}}$ only, owing to a maximum voltage limitation of the test apparatus; in all other specimens data were captured up to $E = 1.5\ \mathrm{MV\,m^{-1}}$. From Fig. 6 the initial dielectric permittivity κ of each specimen is given by the initial slope $\partial D/\partial E$. It is evident that the poling direction has only a slight effect on the magnitude of κ; this is consistent with the fact that the permittivity tensor of poled PZT-5H is close to isotropic. Only slight dielectric non-linearity is evident in the range $0 \le E \le 0.27\ \mathrm{MV\,m^{-1}}$; values of κ for each specimen were estimated by linear regression in this region. This allows the calculation of the change in remnant polarisation ΔP_r for each specimen according to $\Delta P_\mathrm{r} = \Delta D - \kappa E$. The maximum value of ΔP_r in the 180° specimen is approximately twice the saturation polarisation P_sat of the material. Estimating the saturation polarisation in this way gives $P_\mathrm{sat} = 0.24\ \mathrm{C\ m^{-2}}$. The estimated values of ΔP_r can be used to construct yield surfaces corresponding to the onset of ferroelectric transformation. A suitable definition for the yield point in this context is the electric field value E_y at which a fixed value of ΔP_r (the offset) is reached. Electric field yield surfaces for offset values of $\Delta P_\mathrm{r} = 0.01, 0.03$ and $0.10\ \mathrm{C\,m^{-2}}$ (approximately 2, 6 and 20% of the maximum change ΔP_r found in the 180° specimen) are shown in Fig. 7. In each case the full set of specimens $0^\circ \le \theta \le 180^\circ$ in 15° intervals is used and the range $180^\circ < \theta < 360^\circ$ is constructed by symmetry. Note that the 6 and 20% yield surfaces are open: specimens loaded at $\theta < 60^\circ$ did not attain the 20% offset level and those loaded at $\theta < 30^\circ$ did not attain the 6% offset level.

5.1. Calibration of models

Three constitutive models for ferroelectrics have been discussed: a rate-independent self-consistent crystal plasticity model, a simplified viscoplastic crystal plasticity model with a reduced set of transformation systems, and a rate-independent phenomenological

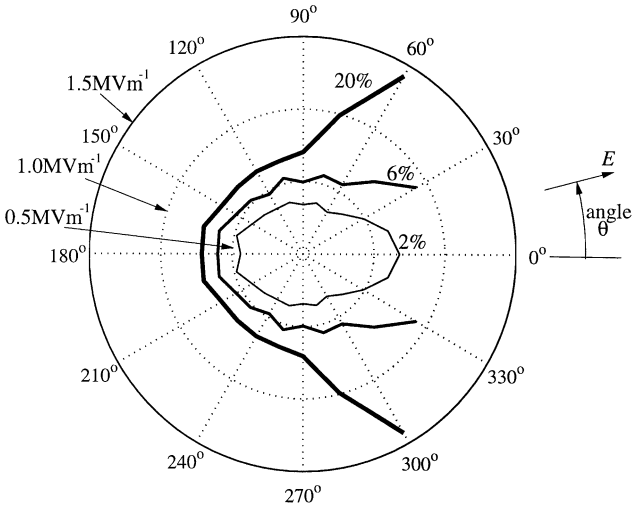

Fig. 7. Measured offset yield surfaces corresponding to 2, 6 and 20% of the maximum change in polarisation (0.48 C m^{-2}) experienced by the 180° specimen. The magnitude of the electric field at yield is plotted against the specimen loading angle θ in polar form.

model. The aim is to simulate the measured data of Figs. 6 and 7 with each model and to use these simulations to assess the ability of each model to capture the multi-axial response of the ferroelectric material. In each case it is necessary to calibrate the model using measurements of material response to fix the model parameters. Here, each model is calibrated by fitting its simulation of the response of the 180° specimen to the measured response shown in Fig. 6 (marked "180°"). This is done by modelling the poling operation from an initially isotropic state, followed by the application of electric field in the opposite direction to the poling direction. The resulting simulations of the response of the 180° specimen are shown in Fig. 8. These curves have been fitted by trial and error, and use the optimised parameters shown in Table 1; subsequent predictions are made using the same set of parameters.

The present modelling problem concerns only the dielectric response; in the simplified viscoplastic model and the phenomenological model, it is not necessary to specify elastic and piezoelectric coefficients. However, with the self-consistent crystal plasticity model, a full set of linear elastic, piezoelectric and dielectric coefficients are required because a fully coupled problem arises in calculating the constraint imposed on each crystal by surrounding material. The dielectric permittivity tensor is close to isotropic and so can be specified sufficiently accurately using one dielectric permittivity κ. The manufacturer's data suggest that the elastic moduli are also close to isotropic and so two elastic moduli (shear modulus μ and Poisson's ratio v) are sufficient. The piezoelectric moduli d_{33}, d_{31} and d_{15} are also specified. Note that these moduli are not measured coefficients for single crystals; instead they have been used as parameters to allow a good quality of fit in Fig. 8. First estimates for these parameters were based on manufacturer's data for the polycrystal. The moduli used to provide a good fit lie within

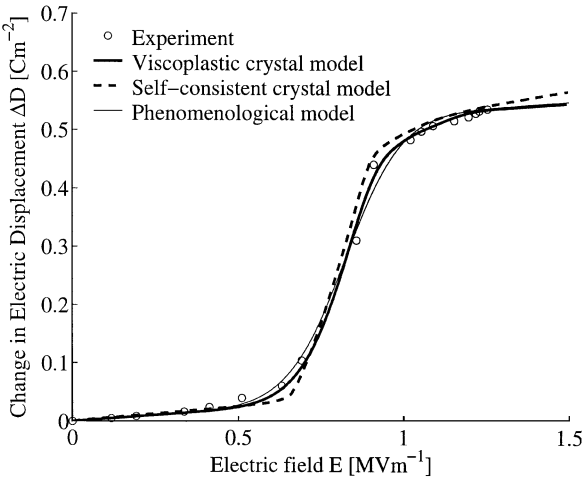

Fig. 8. Measured response of the 180° specimen and fitted simulations using the three models.

a factor of 2 of the measured moduli of the polycrystal. The magnitudes of remnant strain and polarisation for each crystal variant may be estimated from the magnitude of butterfly hysteresis and dielectric hysteresis loops for the material. In particular, the polarisation $|\mathbf{p}_I|$ is about 1.2 times the saturation polarisation of the polycrystal, whilst the remnant strain $\boldsymbol{\varepsilon}_{I(11)}$ (parallel to the polarisation direction) is about 1.8 times the saturation strain reached in the polycrystal. These factors arise because of the distribution of orientations of crystal variants within the polycrystal (see Hwang et al., 1995 for details). The exact values used have been modified by trial and error to provide a good fit to the measured data for the 180° specimen, but remain close to the initial estimates. The critical driving force for switching G_c in the self-consistent crystal plasticity calculation is equal to the product of the electric field at which transformation occurs, and the total polarisation change. By varying G_c whilst keeping $\mathbf{p}_I$ constant, the electric field at which substantial ferroelectric switching occurs in the model can be controlled. Finally, the self-consistent crystal plasticity model of Huber et al. (1999) is a rate-independent formulation; a hardening modulus is required to stabilise the calculation, and to control the slope $\partial D/\partial E$ during ferroelectric switching, as given in Table 1.

5.2. Calculated responses and yield surfaces

Using the parameters of Table 1, electric displacement versus electric field responses were calculated by each of the three models for the set of specimens poled at angles of $0° \leq \theta \leq 180°$ in steps of 15°. Yield surfaces corresponding to 2, 6 and 20% offset polarisation were thereby calculated, following the same procedure as that used in reduction of the measured data. The calculated responses of the 0, 45, 90, 135 and 180° specimens are shown in Fig. 9 (left-hand side) as solid lines. The measured data of Fig. 6 are reproduced (dashed lines) for comparison. The calculated yield surfaces

Table 1
Parameters used in fitting three models to the measured response of the 180° specimen

Parameter	Value
Self-consistent crystal plasticity model	
No. of crystals	205
No. of transformation systems	6150
Shear modulus μ	20.8 GPa
Poisson's ratio ν	0.31
Dielectric permittivity κ	5.8×10^{-8} F m^{-1}
Piezoelectric coefficient d_{33}	2206×10^{-12} V^{-1} m
Piezoelectric coefficient d_{31}	-1103×10^{-12} V^{-1} m
Piezoelectric coefficient d_{15}	2760×10^{-12} V^{-1} m
Remnant strain of variants $\boldsymbol{\varepsilon}_{I(11)}$	1.4%
Remnant polarisation of variants $\lvert\mathbf{p}_I\rvert$	0.5 C m^{-2}
Critical driving force for 90° transformation G_c	0.43 M J m^{-3}
Hardening modulus h	10% G_c
Simplified viscoplastic crystal model	
No. of crystals	5
No. of transformation systems	30
Dielectric permittivity κ	4.2×10^{-8} F m^{-1}
Remnant strain of variants $\boldsymbol{\varepsilon}_{I(11)}$	1.4%
Remnant polarisation of variants $\lvert\mathbf{p}_I\rvert$	0.36 C m^{-2}
Critical driving force for 109° transformation G_c	0.36 M J m^{-3}
Rate constant $\dot{f}_0$	0.040 s^{-1}
Viscoplastic index m	8.0
Saturation index k	1.2
Initial volume fractions c_0	1/4
Phenomenological model	
Dielectric permittivity κ	4.2×10^{-8} F m^{-1}
Yield parameter G_c	0.82 M V m^{-1}
Yield surface shape factor α	0.0011 m^4 C^{-2}
Yield surface shape factor β	0.20 m^4 C^{-2}
Hardening constant h_{0e}	7.14×10^5 F^{-1} m
Hardening constant h_{0s}	620 MPa
Hardening index n_e	1.4
Hardening index n_s	1.4
Tensile saturation strain $2\varepsilon_{sat}$	0.93%
Saturation polarisation P_{sat}	0.24 C m^{-2}

are also shown in Fig. 9 (right-hand side), again as solid lines, with the measured data reproduced from Fig. 7 (dashed lines).

6. Discussion

It is evident from Fig. 8 that all the three models have sufficient flexibility to reproduce the response of the 180° specimen with good accuracy. Next, consider the comparison of the three models with experiment shown in Fig. 9 (left-hand side); here

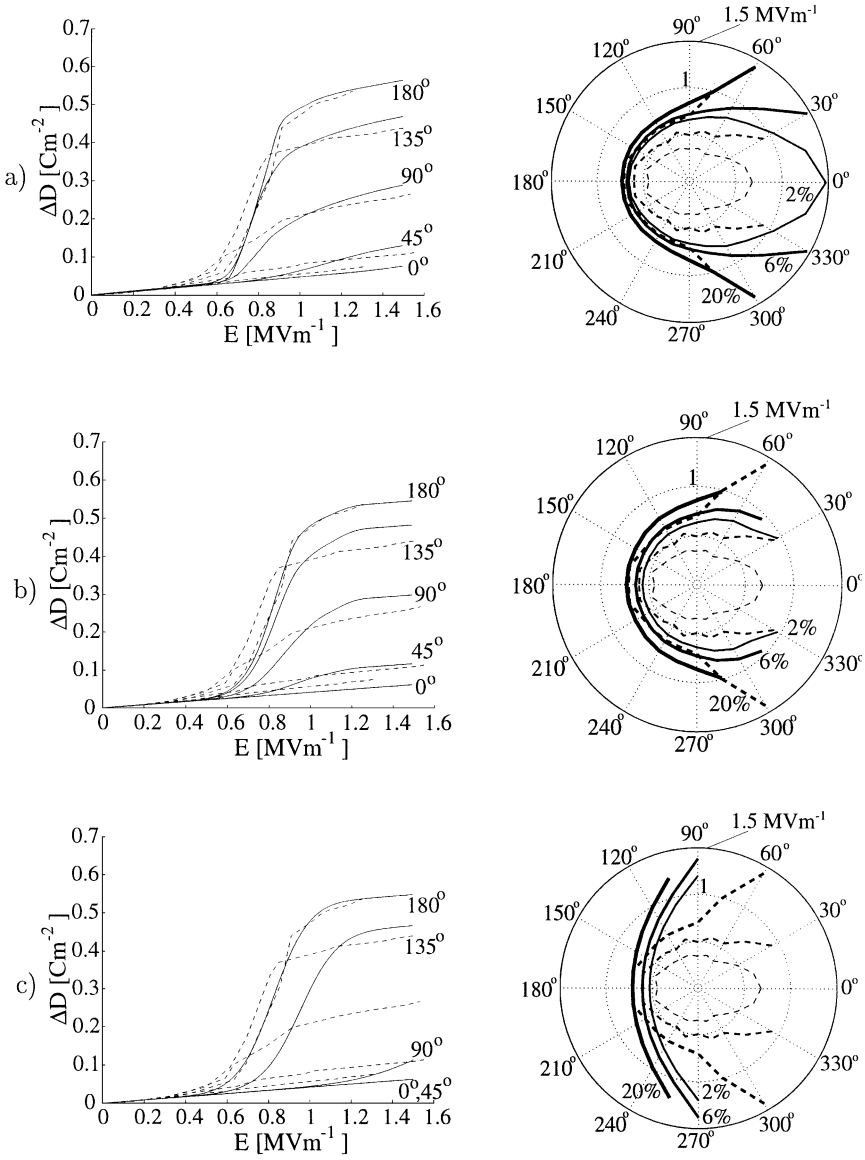

Fig. 9. Calculated responses and yield surfaces (solid lines) using three models: (a) self-consistent crystal plasticity model, (b) simplified viscoplastic crystal model, (c) phenomenological model. The measured data are reproduced (dashed) from Figs. 6 and 7 for comparison.

all the three models also reproduce, at least qualitatively, the gradual reduction in the extent of polarisation switching as angle θ tends towards 0°. In the two crystal plasticity models (Fig. 9a and b) the poling process saturates switching in the 0° direction. In the self-consistent calculation, a small amount of reverse switching may occur during

unloading because of the build up of residual stresses and electric fields resulting from the mismatch in tangent moduli between each crystal and its surroundings. Thus, even in the 0° specimen a small amount of ferroelectric transformation occurs. The simplified crystal plasticity model neglects the interaction of crystals with their surroundings and consequently the 0° response in Fig. 9b is a straight line. In the phenomenological model, the poling process saturates ferroelectric transformation, leaving the material in a 'hard' state. Further ferroelectric switching can then occur only in a direction which takes $\boldsymbol{\varepsilon}_r$ and $\mathbf{P}_r$ away from the saturation condition and thus produces softening. As a result the 0° response in Fig. 9c is also a straight line and at specimen angles close to 0° practically no ferroelectric transformation occurs in the phenomenological model.

Qualitatively, the extent of ferroelectric switching in specimens with $\theta \neq 0^\circ$ is reproduced well by both crystal plasticity models. The internal variables in these two models correspond to volume fractions of crystal variants and are used to keep track of the microstructural state of the polycrystal under multi-axial loading. By contrast, the two tensorial internal variables $(\boldsymbol{\varepsilon}_r, \mathbf{P}_r)$ in the phenomenological model do not keep track of the microstructural state directly; differing states of the volume fraction variables may result in the same state of $(\boldsymbol{\varepsilon}_r, \mathbf{P}_r)$. A more serious defect in the phenomenological model arises as a consequence of the choice of hardening law (22). During poling h_e and h_s become large, resulting in $\dot{\lambda}$ becoming small in Eq. (20). In this saturated condition, the rate of ferroelectric transformation becomes negligible. Compare the predicted responses of the 180 and 90° specimens, as follows. Consider first the 180° specimen, in which loading proceeds with electric field in exactly the opposite direction from the poling field. When the loading point reaches the yield surface, h_e and h_s are initially large, and so there is little transformation. However, each increment in transformation takes the state variables $(\boldsymbol{\varepsilon}_r, \mathbf{P}_r)$ away from saturation, and after a gradual onset, full ferroelectric switching occurs. This allows the 180° response to be reproduced accurately in the phenomenological model. Second, consider the phenomenological model in the case of the 90° specimen. As before, the poling operation leaves h_e and h_s with high values. When the yield surface is reached, the yield surface normals give rise to increments in $\mathbf{P}_r$ and $\boldsymbol{\varepsilon}_r$ which are (roughly) orthogonal to their current values. This is reasonable: for example $\dot{\mathbf{P}}_r$ must follow the direction of the applied field $\mathbf{E}$, at least roughly, for positive dissipation. However, a consequence is that the magnitude of $\mathbf{P}_r$ remains close to P_{sat} and the phenomenological model for the 90° response picks up significant non-linearity only after E reaches about $1.3\,\mathrm{MV\,m^{-1}}$ (see Fig. 9c) — a far greater magnitude of electric field value than that required in either crystal plasticity model, or that found in the measured response. The phenomenological model is thus able to capture well the responses of specimens with θ close to 180°, but its modelling is poor for specimens with $\theta < 120^\circ$.

Next, consider the yield surfaces shown in Fig. 9 (right-hand side). A comparison of the modelled yield surfaces for small offsets (2 and 6%) with experiment provides a severe test for the models; the shapes of these yield surfaces are sensitive to the material response close to the onset of ferroelectric switching. A correct prediction of this part of the response requires accurate prediction of the microstructural state and any residual fields which bias the response. Evidently, none of the three models are able to give accurate predictions of the 2 and 6% yield surfaces. However, there is good

qualitative agreement between model and experiment in the shapes of the 2 and 6% yield surfaces for the self-consistent crystal plasticity model (Fig. 9a). The simplified crystal plasticity model, which makes the assumption of uniform stresses and electric fields captures the shape of the 2 and 6% yield surfaces in the region $|\theta| > 30^\circ$. At angles $|\theta| \leq 30^\circ$ the influence of residual fields on the onset of ferroelectric switching appears to be significant. The late onset of switching in the phenomenological model results in over-estimates of the electric field at yield for 2 and 6% offsets when θ is not close to 180°.

Notice that, in the measured 2% yield surface in Fig. 7, the onset of ferroelectric switching in the 90° specimen is at a *lower* magnitude of electric field than that in the 180° specimen. In fact, specimens in the range 45–135° exhibit this early onset of switching. This effect is not reproduced well by any of the models, although it is just visible in the self-consistent model, since the responses for the 180 and 135° specimens cross in Fig. 9a at $E \approx 0.75$ M V m^{-1}. This feature in the experimental data suggests two possibilities: (i) that there exist ferroelectric transformations with very low coercive fields, which are not active in the 180° specimen, or (ii) residual fields developed during poling act to assist switching towards the 90° direction. The second possibility is consistent with the observation of Lynch (1996) that significant amounts of 90° switching occur during uniaxial electric field loading. This suggests the presence of residual compressive stresses parallel to the poling direction which promote transformations to variants with polarisation close to 90° from the poling direction. Such residual stresses are present in the self-consistent model, although their magnitude is not great enough to give significant effects.

The 20% offset yield surfaces may be described as "collapse" surfaces in the sense that a poled piezoelectric device would suffer a severe change in piezoelectric modulus (of order 40%) under this loading, which could result in loss of function. Both crystal plasticity models reproduce the collapse surface well, with the self-consistent model being the more accurate. Here, again, the ability of these two models to track the microstructural state enables them to make accurate predictions. The experiments revealed that only specimens with $\theta \geq 60^\circ$ reached the 20% offset; thus the fact that the simplified crystal plasticity model neglects residual fields (which is significant in specimens with θ close to 0°) does not affect the predicted collapse surface. Evidently, for high levels of ferroelectric switching the subtle effects of residual fields are swamped by the gross effects of polarisation reorientation.

If poling fully saturates switching, and no reverse transformation occurs during unloading, then a simple expression may be obtained for the maximum change in P_r with loading angle θ. Let the saturation level of remnant polarisation be P_{sat}. From the geometry of switching, the maximum change in P_r reached in loading with an electric field at angle θ is given by $P_{sat}(1-\cos\theta)$. This result provides an estimate of the value of ΔP_r which can be compared with the experimental and model results, provided that P_{sat} is known. For present purposes, we estimate a value of P_{sat} equal to half of the total change in remnant polarisation in the 180° experimental specimen; this matches closely the value of P_{sat} used in the phenomenological model. Fig. 10 shows the maximum values of ΔP_r achieved over the range of angles $\theta = 0$–180° both experimentally and by the three models. The curve $\Delta P_r = P_{sat}(1-\cos\theta)$ is shown as a dashed line

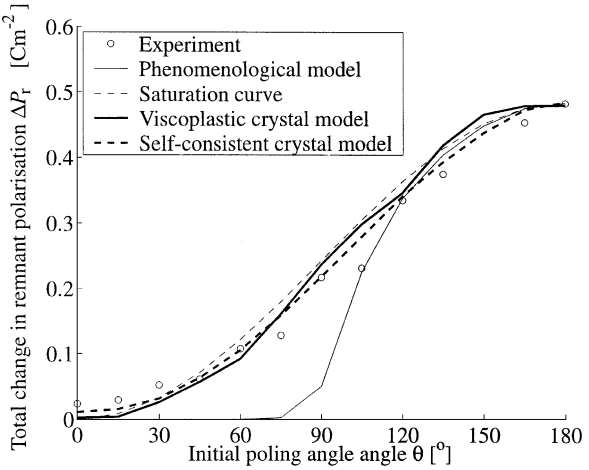

Fig. 10. Maximum values of ΔP_r reached by specimens at poled at various angles θ to the electric field loading direction. Experimental results are marked '○'. The curve $\Delta P_r = P_{sat}(1 - \cos\theta)$ is shown (dashed) for comparison.

in Fig. 10 and is labelled "Saturation curve". The two crystal plasticity models both follow the saturation curve closely, whilst the experimental results lie below the saturation curve, except for the region $\theta \leq 30^\circ$. Note that the self-consistent calculation lies slightly above the saturation curve in this region; this model produces some ferroelectric transformation even in the 0° specimen. The phenomenological model is in good agreement with experiment for angles $\theta \geq 120^\circ$ but is inadequate for predicting the gross change in remnant polarisation for smaller values of θ.

Note that the number of transformation systems included in the simplified viscoplastic crystal model is fewer by a factor of 200 than the number included in the self-consistent calculation. This accounts for the lack of smoothness evident in the results of the viscoplastic calculation in Fig. 10. This difference gives rise to a corresponding improvement in speed of calculation. Furthermore, the self-consistent scheme requires the solution of an implicit linear algebra problem for transformation rates which is solved iteratively, whilst the viscoplastic calculation gives transformation rates directly. The combination of these features gives rise to about three orders of magnitude difference in speed of calculation for the two models, so that the viscoplastic model may be regarded as a rapid and approximate crystal plasticity scheme. Its requirements in terms of memory and processing are comparable to those of the phenomenological model.

7. Conclusions

Three modelling approaches have been developed for the constitutive behaviour of ferroelectric polycrystals. Two of the approaches are based on a crystal plasticity formulation, with the first accounting for the interaction between individual crystals and

their surroundings in a self-consistent way. This self-consistent polycrystal model is able to predict reasonably accurately the response of a ferroelectric polycrystal to multi-axial electric field loading, and reproduces, at least qualitatively, all of the effects seen in the experiment described here. It is well suited to studies of the constitutive behaviour of ferroelectric ceramics. However, for practical engineering modelling, the full self-consistent calculation is computationally cumbersome. An improvement of some three orders of magnitude in speed can be made by neglecting local interaction fields, by simplifying the set of crystal transformation systems modelled, and by assuming viscoplastic behaviour. This large improvement in speed is accompanied by a small loss of accuracy, combined with the loss of some of the more subtle features of material behaviour. However the main features of switching are well represented in the simplified crystal plasticity model. A third modelling approach, based on phenomenological theory, is suitable for loading which is close to uniaxial, and can be used in applications involving cyclic uniaxial loading, where rapid estimates of material response are needed. This model is unable, in its present form, to reproduce the full range of multi-axial behaviour. However, improvements in the performance of the phenomenological model can be made, at the cost of increased complexity. In particular, the choice of an appropriate hardening rule for use under multi-axial loading conditions remains an open question, requiring further experiments. We conclude that the simplified crystal plasticity model presented here gives a sufficient trade-off between speed and accuracy to be of use as a practical engineering tool.

Acknowledgements

The authors wish to acknowledge the contributions of Prof. A.C.F. Cocks, Prof. R.M. McMeeking, and C.M. Landis through useful discussions. The work of J.E.H. is supported by the E.P.S.R.C.

References

Arlt, G., 1996. A physical model for hysteresis curves of ferroelectric ceramics. Ferroelectrics 189, 103–119.

Bassiouny, E., Ghaleb, A.F., Maugin, G.A., 1988a. Thermodynamical formulation for coupled electromechanical hysteresis effects — I. Basic equations. Int. J. Engng. Sci. 26 (12), 1279–1295.

Bassiouny, E., Ghaleb, A.F., Maugin, G.A., 1988b. Thermodynamical formulation for coupled electromechanical hysteresis effects — II. Poling of ceramics. Int. J. Engng. Sci. 26 (12), 1297–1306.

Bassiouny, E., Maugin, G.A., 1989a. Thermodynamical formulation for coupled electromechanical hysteresis effects — III. Parameter identification. Int. J. Engng. Sci. 27 (8), 975–987.

Bassiouny, E., Maugin, G.A., 1989b. Thermodynamical formulation for coupled electromechanical hysteresis effects — IV. Combined electromechanical loading. Int. J. Engng. Sci. 27 (8), 989–1000.

Cao, H., Evans, A.G., 1993. Non-linear deformation of ferroelectric ceramics. J. Am. Ceramic Soc. 76 (4), 890–896.

Chen, P.J., 1980. Three dimensional dynamic electromechanical constitutive relations for ferroelectric materials. Int. J. Solids Struct. 16, 1059–1067.

Chen, P.J., Madsen, M.M., 1981. One dimensional polar responses of the electrooptic ceramic PLZT 7/65/35 due to domain switching. Acta Mech. 41, 255–264.

Chen, W., Lynch, C.S., 1998a. A micro-electro-mechanical model for polarization switching of ferroelectric materials. Acta Mater. 46 (15), 5303–5311.

Chen, W., Lynch, C.S., 1998b. A model for simulating polarization switching and AF–F phase changes in ferroelectric ceramics. J. Intell. Mater. Systems Struct. 9 (6), 427–431.

Chen, X., Fang, D.N., Hwang, K.C., 1997. Micromechanics simulation of ferroelectric polarization switching. Acta Mater. 45 (8), 3181–3189.

Cocks, A.C.F., McMeeking, R.M., 1999. A phenomenological constitutive law for the behaviour of ferroelectric ceramics. Ferroelectrics 228, 219–228.

Fan, J., Stoll, W.A., Lynch, C.S., 1999. Nonlinear constitutive behaviour of soft and hard PZT: experiments and modeling. Acta Mater. 47 (17), 4415–4425.

Huber, J.E., 1998. Ferroelectrics: models and applications. Ph.D. Thesis, University of Cambridge.

Huber, J.E., Fleck, N.A., Landis, C.M., McMeeking, R.M., 1999. A constitutive model for ferroelectric polycrystals. J. Mech. Phys. Solids 47, 1663–1697.

Hwang, S.C., Huber, J.E., McMeeking, R.M., Fleck, N.A., 1998. The simulation of switching in polycrystalline ferroelectric ceramics. J. Appl. Phys. 84 (3), 1530–1540.

Hwang, S.C., Lynch, C.S., McMeeking, R.M., 1995. Ferroelectric/ferroelastic interactions and a polarization switching model. Acta Metall. Mater. 43 (5), 2073–2084.

Kamlah, M., Böhle, U., 2001. Finite element analysis of piezoceramic components taking into account ferroelectric hysteresis behavior. Int. J. Solids Struct., in press.

Kamlah, M., Tsakmakis, C., 1999. Phenomenological modeling of the non-linear electro-mechanical coupling in ferroelectrics. Int. J. Solids Struct. 36, 669–695.

Landis, C.M., McMeeking, R.M., 1999. A phenomenological constitutive law for ferroelastic switching and a resulting asymptotic crack tip solution. J. Intell. Mater. Systems Struct. 10, 155–163.

Lynch, C.S., 1996. The effect of uniaxial stress on the electro-mechanical response of 8/65/35 PLZT. Acta Mater. 44 (10), 4137–4148.

Lynch, C.S., 1998. On the development of multiaxial phenomenological constitutive laws for ferroelectric ceramics. J. Intell. Mater. Systems Struct. 9, 555–563.

Pierce, D., Shih, C.F., Needleman, A., 1984. A tangent modulus method for rate dependent solids. Comput. Struct. 18 (5), 875–887.